Journal of Catalysis 272 (2010) 298–308

Contents lists available at ScienceDirect

Journal of Catalysis

journal homepage: www.elsevier.com/locate/jcat

Influence of layer structure preservation on the catalytic properties of the pillared zeolite MCM-36

Sudeep Maheshwari [a,1], Cristina Martínez [b,1], M. Teresa Portilla [b], Francisco J. Llopis [c], Avelino Corma [b,*], Michael Tsapatsis [a,**]

[a] Department of Chemical Engineering and Materials Science, University of Minnesota, Minneapolis, Minnesota, USA
[b] Instituto de Tecnología Química (UPV-CSIC), Universidad Politécnica de Valencia, Consejo Superior de Investigaciones Científicas, Valencia, Spain
[c] Departamento Ingeniería Química, U.V.E.G. Universidad de Valencia, Burjassot, Valencia, Spain

ARTICLE INFO

Article history:
Received 3 December 2009
Revised 4 April 2010
Accepted 14 April 2010
Available online 14 May 2010

Keywords:
Swelling
Pillaring
MWW zeolite
MCM-36
Layered zeolites
Xylene isomerization
Alkylation
Cracking

ABSTRACT

MCM-36 is a catalytically active material made by swelling and subsequent pillaring of a layered zeolite precursor, MCM-22(P). However, the swelling procedures lead to significant destruction of layer structure and alteration of framework silicon/aluminum (Si/Al) ratio, which are likely to influence the acidity and catalytic activity of the final materials. We report a milder swelling and pillaring process to prevent such structural destruction. The resulting pillared materials show higher crystallinity and improved retention of the zeolitic layer structure when compared to the ones prepared by the previously reported methods involving more aggressive treatments. Implications of such structural preservation on the physicochemical, acidic and catalytic properties of the materials have been investigated using a variety of characterization methods. The milder swelling results in catalytic materials with stronger acid sites and, at similar Si/Al ratios, higher acid site density and higher catalytic activity when compared to the MCM-36 materials produced using the previously reported more aggressive swelling process.

1. Introduction

MCM-36 [1] is the first pillared material with zeolitic layers [2,3]. It is derived from a layered precursor, MCM-22(P). The layers of MCM-22(P) are intercalated by silica species, which convert into inorganic pillars upon polymerization and hold the layers apart creating interlayer mesoporous spaces [4]. These mesopores allow increased access to protonic sites present on the zeolite, making this material attractive for catalytic and sorption applications [2]. The beneficial effect of pillaring can be seen from the high catalytic activity of MCM-36 when compared to its non-pillared counterpart MCM-22 for a variety of reactions such as vacuum gasoil cracking [5], alkylation of isoparaffins or aromatics [6], etc.

Synthesis of MCM-36 from MCM-22(P) is a two-step process [1,4,6,7]. In the first step, MCM-22(P) is swollen by cetyltrimethylammonium cations in the presence of a base (pH > 13.5) at elevated temperature (353–373 K). The swollen MCM-22(P) is then pillared with tetraethoxysilane (TEOS) derived silica.

Earlier [8–10] and more recent [11] reports have shown that the swelling process results in significant destruction of zeolite structure with dissolution of framework silica, dealumination of the material and reduction in microporosity within the zeolite layers. This is likely to affect the density and nature (both strength and accessibility) of protonic sites, which in turn, will influence the catalytic activity of the MCM-36 materials. The change in pore structure can also influence the selectivity [5,12–14].

Recently, we reported an alternative procedure to swell MCM-22(P), which results in preservation of the layer and pore structure and of the zeolite composition [11]. Use of lower temperature for swelling was the key to prevent the structural destruction and dissolution of the precursor. The resultant swollen material could be pillared to make an analog of MCM-36, albeit with much improved crystallinity.

In this work, a detailed study describing the effect of swelling conditions on the physiochemical properties and catalytic behavior of MCM-36 materials is presented. X-ray diffraction (XRD), transmission electron microscopy (TEM), nuclear magnetic resonance (NMR), nitrogen adsorption and IR spectroscopy of adsorbed pyridine were used to characterize the structural and acid site differences in pillared materials prepared using two different swelling conditions. The catalytic activity of these materials for a particular

* Corresponding author. Fax: +34 96 3879444.
** Corresponding author. Fax: +1 (612) 626 7246.
E-mail addresses: acorma@itq.upv.es (A. Corma), tsapatsi@cems.umn.edu (M. Tsapatsis).
[1] Equally contributed authors.

0021-9517/$ - see front matter © 2010 Elsevier Inc. All rights reserved.
doi:10.1016/j.jcat.2010.04.011

set of reactions was tested. It is shown that for given silicon to aluminum ratio (Si/Al), MCM-36 materials prepared by milder swelling exhibit stronger acidity and higher catalytic activity.

2. Experimental

Three different MCM-36 samples were prepared in this study. Two samples were prepared starting from the same MCM-22(P) precursor but with different swelling conditions to assess the effect of swelling on the Si/Al ratio, morphology and structure of the pillared materials. Different swelling conditions were found to result in significant difference of Si/Al ratio in the final materials. Therefore, a third sample was made starting with a different precursor to match the final Si/Al ratio of the pillared material exhibiting the lower ratio. The details of precursor synthesis, swelling and pillaring procedures are described below.

2.1. Synthesis of MCM-22(P)

Two MCM-22(P) batches with different Si/Al ratios were synthesized using the method of Corma et al. [5,15]. For the MCM-22 precursor with Si/Al ~ 45 (gel composition), 0.54 g of sodium aluminate (MP biomedicals, USA) and 1.86 g of sodium hydroxide (97+%, Fisher) were dissolved in 233.06 g of distilled water. Subsequently, 14.34 g of hexamethyleneimine (HMI) (Aldrich) and 17.68 g of fumed silica (Cab-o-sil M5) were added to the mixture. The mixture was allowed to stir for 5 h at room temperature, followed by 11 days in rotating Teflon-lined steel autoclaves at 408 K. The crystalline product obtained after 11 days was collected by centrifugation and repeatedly washed with distilled water to reduce the pH to 9.

For the precursor with Si/Al ~ 20, the amounts of sodium aluminate and sodium hydroxide were changed to 1.37 g and 1.32 g, respectively, and the mixture was stirred for 20 h at room temperature before heating it to 408 K.

2.2. Swelling and pillaring of MCM-22(P)

Both precursors were swollen with cetyltrimethylammonium bromide (CTAB) at room temperature under high pH conditions. The composition of the swelling mixture was the same as the one reported by Kresge [1] and Corma [5]. Typically, 9 g of aqueous slurry of MCM-22(P) (20 wt.% solids) was mixed with 35 g of an aqueous solution of 29 wt.% CTAB (Aldrich) and 11 g of an aqueous solution of 40 wt.% TPAOH (Alfa Aesar). The pH of the resulting mixture was ~13.8. The mixture was allowed to stir for 16 h at room temperature, after which, the particles were recovered by repeated cycles of centrifugation and washing with DI water (10-min centrifugation at 10,000 rpm and redispersion in fresh water). The process of centrifugation and washing was repeated until the 002 and 003 reflections were detected in the XRD patterns [11]. A portion of MCM-22(P) with Si/Al ~ 45 was also swollen at 353 K following the procedure reported by Corma et al. [5,15] for comparison.

Pillaring of the swollen materials was performed according to the procedure reported by Barth et al. [7]. Typically, 1 g of swollen MCM-22(P) powder was mixed with 5 g of TEOS (tetraethoxysilane, Fluka), stirred for 25 h at 351 K under argon atmosphere, then filtered and dried at room temperature. Of the resulting solid, 0.5 g was hydrolyzed in 5 g of water (pH ~ 8, controlled with NaOH) for 6 h at 313 K, then filtered, dried at 300 K and calcined at 723 K under N_2 flow (140 ml min^{-1}) for 6 h and finally at 823 K in air for 12 h (temperature ramp rate of 2 K/min).

2.3. Characterization methods

The silicon and aluminum contents of the pillared materials were determined using a 715-ES inductive coupled plasma (ICP) optical emission spectrometer.

Nitrogen adsorption–desorption measurements were carried out at 77 K with an Autosorb-1 analyzer (Quantachrome Instruments). Prior to the measurement, samples were evacuated overnight at 623 K and 1 mm Hg. The specific surface area and pore size distribution were calculated by applying the BET and BJH models, respectively, to the nitrogen adsorption data.

Powder X-ray diffraction (XRD) patterns were collected on a Bruker AXS D5005 diffractometer using Cu Kα radiation. Data were collected in the 2θ range from 1° to 30° with a step size of 0.04° and a step time of 3 s.

All NMR spectra were recorded at a field of 11.7 T (BRUKER Avance 500). ^{29}Si MAS NMR spectra were recorded at 99.37 MHz using 4 mm rotors at a spinning speed of 8 kHz, a dwell time of 16.65 μs, a $\pi/2$ pulse of 4.0 μs and a recycle delay of 60 s. All spectra were referenced with respect to tetramethylsilane (0 ppm). ^{27}Al MAS NMR spectra were recorded at 130.34 MHz using 4 mm rotors at 14 kHz spinning speed, a dwell time of 0.5 μs, a selective $\pi/18$ pulse of 0.3 μs and a recycle delay of 0.1 s. An aqueous solution of aluminum sulfate (0.1 M) was used as the reference (0 ppm).

A FEI Tecnai G2 F30 transmission electron microscope (TEM) equipped with a charge couple device (CCD) and operated at 300 kV was used for direct imaging of pillared materials. Samples were prepared by dispersing powders in water and placing a few drops of the dispersion on a carbon-coated copper grid followed by air drying to evaporate off the water.

The concentration of acidic sites in various samples was obtained by FT–IR spectroscopy using pyridine as the probe molecule. Pyridine adsorption–desorption experiments were carried out on self-supported wafers (10 mg cm^{-1}) of original samples previously activated at 673 K and 10^{-2} Pa for 2 h. After wafer activation, the base spectrum was recorded, and pyridine vapors (6.5×10^2 Pa) were admitted into the vacuum IR cell and adsorbed onto the zeolite at 423 K. Desorption of pyridine was performed in vacuum over three consecutive 1h periods of heating at 423, 523 and 623 K, each followed by an IR measurement at room temperature. All the spectra were scaled according to the sample weight. The number of acid sites was calculated from the intensity of the band at 1450 cm^{-1} (Lewis acid sites) and 1550 cm^{-1} (Brønsted acid sites) by applying the extinction coefficients from Emeis [16]:

$$C_B = 1.88 \cdot IA_B \cdot R^2/W$$

and

$$C_L = 1.42 \cdot IA_L \cdot R^2/W$$

where B represents Brønsted acid center, L represents Lewis acid center, C is the concentration (mmol pyridine/g catalyst), IA is the integrated absorbance, R is the radius of the catalyst disk (cm), and W is the weight of the disk (mg).

2.4. Catalytic testing

Catalytic cracking of n-decane and vacuum gasoil (VGO, Table 1) was performed in an automated microactivity test (MAT) unit, which can be operated in a continuous way up to eight cycles, i.e., stripping–reaction–regeneration, without operator intervention. The reaction zone and product recovery system have been designed in accordance with ASTM D-3907. In order to vary the conversion, the catalyst to oil ratio was varied in the range of 0.25–0.83 g g^{-1} by keeping the amount of catalyst constant (0.5 g) and changing the amount of feed. Before each experiment,

Table 1
Vacuum gasoil properties.

Density (15 °C) g cc^{-1}					0.916
Aniline point (°C)					79.2
K (UOP)					11.82
Sulfur (wt.%)					1.65
Nitrogen (ppm)					1261
Na (ppm)					0.18
Cu (ppm)					<0.1
Fe (ppm)					0.3
Ni (ppm)					0.2
V (ppm)					0.4
Average molecular weight					407
Aromatic carbon (ndM) (%)					22.96
Naphthenic carbon (ndM) (%)					15.16
Paraffinic carbon (ndM) (%)					61.88
Aromatic rings/molecule (ndM)					1.17
Naphthenic rings/molecule (ndM)					1.01
Distillation curve ASTM D-1160 (°C)					
5%	10%	30%	50%	70%	90%
319	352	414	436	459	512

the system was purged with a 30 cc/min N_2 flow for 30 min at the reaction temperature. After reaction, stripping of the catalyst was carried out for 15 min using a N_2 flow of 30 cc/min. During the reaction and stripping steps, the liquid products were collected in the corresponding glass receivers located at the exit of the reactor, kept at 280 K by means of a computer-controlled bath. Meanwhile, the gaseous products were collected in a gas burette by water displacement. After stripping, the catalyst was regenerated at 813 K for 3 h, in a 100 cc/min stream of air. Catalytic cracking reaction was performed at 773 K and 60 s time on stream (TOS) for both feedstocks. The gases were analyzed using a Varian 3600 GC equipped with two detectors, a thermal conductivity detector (TCD) for analysis of H_2 and N_2, which were separated in a 15 m molecular sieve column, and a flame ionization detector (FID) for C1–C6 hydrocarbons separated in a 30 m Plot/Al_2O_3 column. In the case of *n*-decane cracking, the liquids were analyzed in a Varian 3900 GC with a 100 m, 0.25 mm ID Petrocol DH column, and in the case of gasoil by simulated distillation (SIMDIS) in a Varian 3800 GC equipped with a 10 m, 0.53 mm ID MXT-2887 metal column supplied by Restek Corp. and using the STARD SD software from Varian following the ASTM D-2887 standard. The CO_2 formed during the regeneration step is monitored and quantified by means of an IR cell (Rosemund Binos-100). More details can be found in [17].

The meta-xylene isomerization and benzene and toluene alkylation reactions were conducted in a fixed-bed continuous glass down-flow reactor (11 mm internal diameter). The catalyst was diluted with glass and placed in the reactor bed.

The meta-xylene isomerization was carried out with a meta-xylene/N_2 molar ratio of 1:4. In the alkylation reaction, benzene or toluene was fed in excess to alcohol in a molar ratio of 4:1, while the N_2 flow was fixed to achieve a 10:1 M ratio of N_2 to alcohol. Prior to addition of the reactants, the catalyst was heated to 623 K at a heating rate of 5 K/min, under a flow of nitrogen. After 30 min, the temperature was raised to 723 K and kept at that temperature for 1 h. The reactor was then cooled to reaction temperature: 623 K for meta-xylene isomerization and 553 K for aromatics alkylation. When the temperature was stabilized, the reactants in liquid-phase were fed at the top of the reactor. The reactor exit was connected to a multisampling controlled heated valve equipped with a hydrocarbon detector at the outlet, in order to detect the moment when the products fill the first loop. This moment is considered the zero reaction time, and the gas sample is kept in the first loop. The rest of the loops were automatically filled at preprogrammed times on stream (10, 30, 60, 180 and 360 s). The products of the reactions were analyzed in a gas chromatograph (HP5890II) equipped with a Supelco-WAX10 capillary column (60 m length, 0.2 mm inner diameter) and a flame ionization detector. Initial rates and selectivities were calculated as detailed elsewhere [18].

3. Results and discussion

3.1. Si/Al ratio and surface area

The physicochemical properties of the three samples are listed in Table 2. The sample name indicates the preparation condition and final Si/Al ratio of the pillared material. For example, MCM36-RT-23 indicates that the sample was prepared by swelling at room temperature (RT) and the final Si/Al ratio in the pillared material is 23. HT stands for high temperature (353 K).

Samples MCM36-RT-54 and MCM36-HT-24 were prepared starting from the same MCM-22(P), but swelling at room temperature and 353 K, respectively. It can be seen that swelling at high temperature (which is the usual procedure reported in the literature) results in considerable dissolution of framework silica due to the reactive basic conditions. The resulting material (MCM36-HT-24) has a lower Si/Al ratio when compared to the precursor despite the silica incorporation during the pillaring process. Swelling at room temperature prevents framework silica dissolution to a great extent. The final pillared materials (MCM36-RT) have higher Si/Al ratio than the corresponding precursor materials, as expected, due to incorporation of silica during the pillaring process.

Nitrogen adsorption/desorption isotherms of the three pillared samples are shown in Fig. 1. An increase in the adsorption volume up to relative pressures of ~0.3 indicates the presence of mesopores created by pillaring in all three samples. However, the increase in adsorption volume continues to higher pressure values in sample MCM36-HT-24, indicating the presence of larger mesopores as well as a wider pore size distribution. As already observed from decrease in the Si/Al ratio, MCM36-HT-24 is produced following significant dissolution of framework silica. Such dissolution is likely to create secondary pore structure with larger mesopores in addition to the ones produced by pillaring. The BJH pore size dis-

Table 2
Physicochemical properties of MCM36 samples.

Sample	Si/Al in precursor gel	Si/Al (ICP)	S_{BET} (m^2/g)
MCM36-RT-54	45	54	789
MCM36-HT-24	45	24	862
MCM36-RT-23	20	23	742

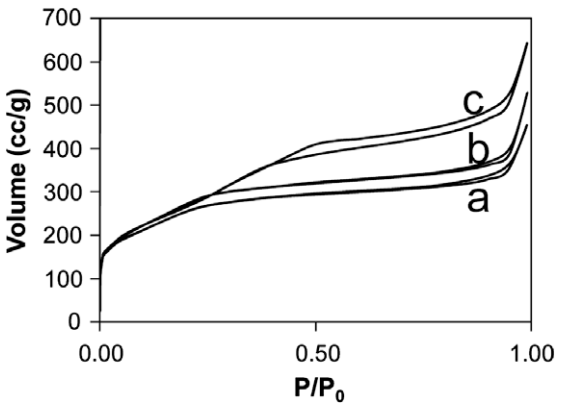

Fig. 1. Nitrogen adsorption isotherms for (a) MCM36-RT-23, (b) MCM36-RT-54 and (c) MCM36-HT-24.

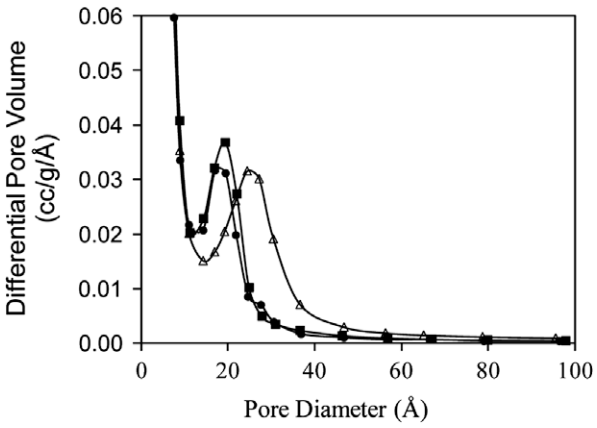

Fig. 2. BJH pore size distribution of MCM36-RT-23 (●), MCM36-RT-54 (■) and MCM36-HT-24 (Δ).

tribution shown in Fig. 2 clearly shows that MCM36-HT-24 has bigger mesopores (~2.7 nm) when compared to the two MCM36-RT samples (~1.8 nm). It is important to remark that the initial Si/Al ratio of the precursor is not affecting the room temperature swelling procedure and that both samples, MCM36-RT-54 and MCM36-RT-23, have similar textural properties and a narrow mesopore size distribution.

Surface areas of all three samples were estimated by applying the BET method to the nitrogen adsorption isotherms shown above, and values are reported in Table 2. The two MCM-36 samples prepared via room temperature swelling (MCM36-RT-54 and MCM36-RT-23) show very similar BET surface areas. The values reported are typical of pillared MCM-36 materials [6]. MCM36-HT-24 has the highest surface area among the three samples, presumably due to creation of secondary pore structure by dissolution of framework silica as well as severe fragmentation during the high-temperature swelling process [11].

3.2. X-ray diffraction

X-ray diffractograms of the three samples are shown in Fig. 3. The samples show a 001 peak around $2\theta \sim 2^\circ$ corresponding to an interlayer distance of about 4.5 nm, which indicates successful pillaring [1,3,6]. However, the materials prepared by room temperature swelling (traces a and b) show much sharper peaks and higher order reflections (002 and 003) when compared to the one prepared by high-temperature swelling (trace c). These observations indicate a higher crystallinity, better structural preservation, and long-range ordering of layers in the two MCM36-RT samples and are in agreement with the physicochemical properties discussed above. Again, no major qualitative differences are observed for the materials prepared by RT swelling starting from the two different precursors.

3.3. Transmission electron microscopy

Transmission electron microscopy was employed for the direct visualization of crystal morphology and layer structure. The starting MCM-22(P) material consists of thin circular disks that are about 500–1000 nm in diameter and 50–100 nm in thickness (images not shown) [11]. TEM images of MCM36-RT-54 and MCM36-HT-24 are shown in Fig. 4 for comparison. MCM36-RT-54 shows a remarkable preservation of crystal morphology during the swelling and pillaring process. The crystals retain their circular disk morphology and sharp facets as seen in Fig. 4a (the crystals are oriented along their thinner edge in this image). Fig. 4b shows a higher resolution image of the same sample. Stacks of MWW layers can be seen in each crystal (appearing as dark bands separated by white bands corresponding to gallery space). The long-range ordering of layers, suggested by the presence of higher order reflections in the XRD patterns, can be directly visualized in this micrograph. The remarkable ordering of the layers suggests a nearly perfect pillaring of material, without major changes to the crystal morphology. The interlayer spacing calculated from these TEM images is in agreement with those obtained from XRD. Images of MCM36-RT-23 sample show similar structural properties (not shown).

MCM36-HT-24, on the other hand, shows a highly disordered structure (Fig. 4c). The disk-like morphology and sharp crystal facets are no longer visible. Unlike MCM36-RT-54 that showed ordered stacks of layers throughout the sample, this material shows small domains of stacked layers surrounded by disordered amorphous domains (Fig. 4d). It appears that swelling and pillaring in this sample proceeds with considerable fragmentation and partial dissolution of crystals, destroying the overall morphology and creating disordered domains. Note that the only difference in the preparation of this sample when compared to MCM36-RT-54 is the temperature of swelling and subsequent water washings. Thus, room temperature swelling results in a well-ordered pillared material with remarkable structural preservation.

3.4. Multinuclear solid-state NMR investigation

Solid-state NMR was employed to understand the effect of swelling conditions on the local bonding environment in the pillared materials. Fig. 5, trace a, shows the ^{29}Si NMR spectra of

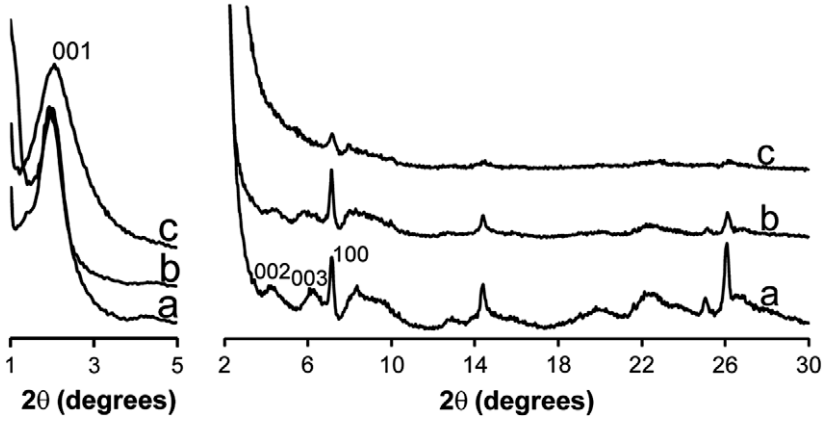

Fig. 3. XRD patterns from the three pillared materials: (a) MCM36-RT-23, (b) MCM36-RT-54 and (c) MCM36-HT-24. The figure has been divided into two parts for better visualization of 0 0 1 peak and traces have been shifted vertically for clarity.

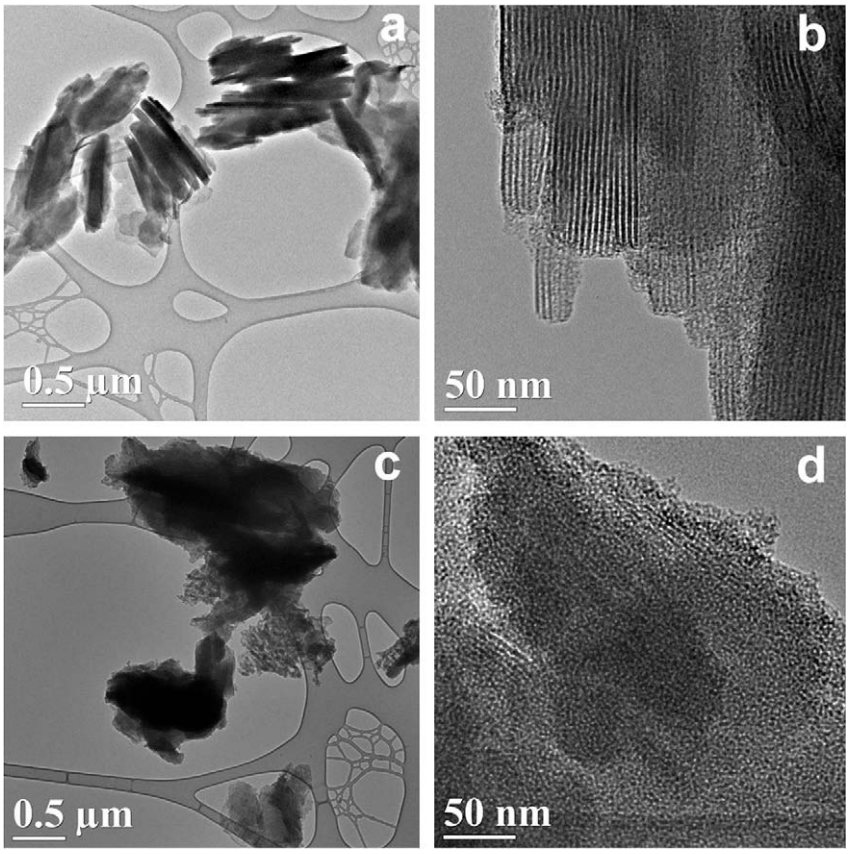

Fig. 4. TEM images of MCM36-RT-54 (a and b) and MCM36-HT-24 (c and d) at various magnifications.

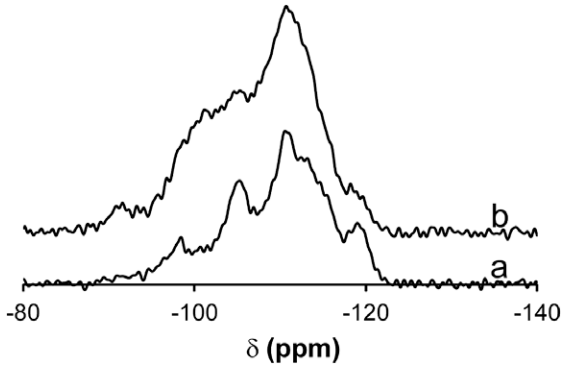

Fig. 5. ^{29}Si MAS NMR spectra of (a) MCM36-RT-23 and (b) MCM36-HT-24.

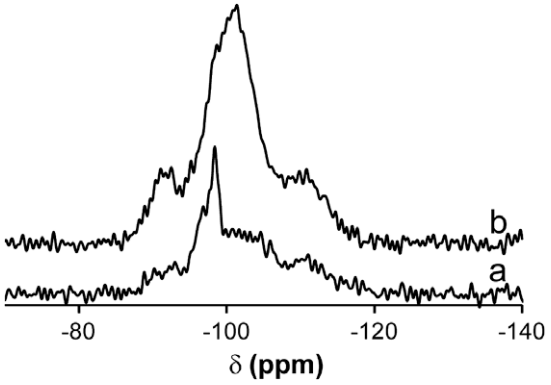

Fig. 6. ^{29}Si CP MAS NMR spectra of (a) MCM36-RT-23 and (b) MCM36-HT-24.

MCM36-RT-23. Three well-resolved peaks (at −104, −110, −119 ppm) along with two less resolved shoulders (around −113 and −116 ppm) can be seen in the −104 to −120 ppm range, which correspond to crystallographically non-equivalent Q^4 tetrahedral sites (Q^n stands for $X_{4-n}Si[OSi]_n$) [19–22]. A small peak around −98 ppm is attributed to Q^3 sites [23,24] arising from the silanol groups on the MWW layer surface as well as those present on the silica pillars. The overall spectrum is very similar to the one obtained from an MWW structure (e.g., MCM-22) [19–22], suggesting that the local bonding environment stays well preserved in this material.

The spectrum of MCM36-HT-24 (Fig. 5, trace b) appears very different. The peaks are much broader and less resolved, indicating a large dispersion in the local bonding environment. A broad shoulder can be seen around the −100 ppm range, indicating a high concentration of Q^3 species. This is most likely due to the structural destruction during the swelling process (as already suggested by the decrease in Si/Al ratio and partial dissolution of zeolite crystals noted in TEM images) that results in bond breaking around Q^4 sites creating Q^3 sites.

^{29}Si CP MAS NMR spectra of the two pillared materials are shown in Fig. 6. Both materials show an intense peak around −98 to −100 ppm range, corresponding to the Q^3 silanol species [23,24]. The Q^3 and Q^2 species are more rapidly polarized than the Q^4 species in CP mode due to their closer proximity to the silanols and give intense peaks [25]. However, this peak is much broader in MCM36-HT-24 sample. This could be indicative of different types of silanol groups present in this sample (e.g., silanol groups on cups of MWW layers, silanol groups created by breaking of Si–O–Si bonds around other Q^4 species). The same peak in

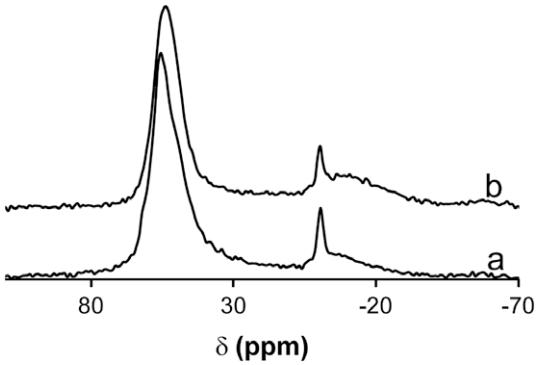

Fig. 7. ^{27}Al MAS NMR spectra of (a) MCM36-RT-23 and (b) MCM36-HT-24.

MCM36-RT-23 sample is very sharp, indicative of a single type of silanol species (most likely the ones present on the cups of MWW layers). A peak around −90 ppm is also visible in both samples, which arises due to the Q^2 species [19,20] created by Si–O–Si bond breaking during swelling or pillaring step. This peak is more intense in MCM36-HT-24 indicative of greater bond breaking.

^{27}Al NMR results for the pillared materials are shown in Fig. 7. The peak at 55 ppm in both samples is due to the framework aluminum [22,23], while a small peak around 0 ppm is due to the extraframework aluminum, known to be created by dealumination during calcination of the samples [23].

3.5. Acidic properties of pillared materials

So far, we discussed the effect of swelling conditions on the physiochemical and structural properties of resulting pillared materials. It was found that swelling at high temperature results in significant dissolution of framework silica and greater destruction of crystal structure. These changes are likely to affect the acidity and catalytic properties of the samples.

The acidic properties of all three samples were evaluated using infrared spectroscopy following pyridine adsorption. The results are summarized in Table 3. MCM36-RT-54 and MCM36-HT-24, although prepared from the same MWW precursor, present very different acidity due to significant desilication of the latter sample. The sample prepared by high-temperature swelling (MCM36-HT-24) shows slightly lesser number of total Brønsted acid sites (at 423 K) as well as lower amount of strongest Brønsted acid sites (at 623 K), when compared with the pillared material prepared via room temperature swelling (MCM36-RT-54). Such a reduction in Brønsted acidity due to desilication has been reported for several zeolites [26–28].

Since Si/Al ratio plays a deciding role in the final concentration of acidic sites in zeolites, it is interesting to compare the two pillared materials with similar Si/Al ratio obtained using different swelling conditions, MCM36-RT-23 and MCM36-HT-24. It can be easily seen that at a given Si/Al ratio in the final pillared material, the room temperature swelling procedure gives a sample with much higher concentration of Brønsted acid sites and with a higher proportion of sites with medium-to-strong acidity. This result is important from the catalytic point of view, since activity and selectivity of the catalyst will be related to the total number of Brønsted acid sites and their acid strength distribution. MCM36-RT-54 has a lower number of total Brønsted acid sites, in agreement with its lower Al content, but the proportion of stronger acid sites, i.e., those able to retain pyridine at 623 K, is high and comparable to that measured for MCM36-RT-23 (see Table 3).

On the other hand, MCM36-HT-24 has significantly more Lewis acid sites, suggesting larger amount of extraframework Al species created by some dealumination of the material during the high-temperature swelling. This is in contrast with the ^{27}Al MAS NMR spectra (Fig. 7) that show similar amounts of extraframework Al species (at 0 ppm) for both samples. Miltenburg et. al. [27] reported a similar observation upon alkali treatment of MCM-22 zeolite, which resulted in increase in the Lewis acid sites without any changes in the ^{27}Al NMR spectra when compared to the parent zeolite. Previous reports indicate that ^{27}Al NMR can sometimes underestimate the amount of extraframework Al species if they are in a highly distorted coordination [29]. These Al species are not detected in NMR and are often referred to as 'NMR silent' or 'invisible aluminum' in the zeolite literature [30]. Presence of such, 'NMR silent,' extraframework aluminum in MCM36-HT-24 can be the reason for the observed discrepancy in acidity and NMR results.

Table 3
Acidity as determined by FT–IR combined with pyridine adsorption at various temperatures.

Sample	Acidity (μmol pyridine/g)						
	Brønsted			B623/B423	Lewis		
	423 K	523 K	623 K		423 K	523 K	623 K
MCM36-RT-54	56	50	33	0.60	19	17	17
MCM36-HT-24	62	47	21	0.34	61	44	42
MCM36-RT-23	108	98	65	0.60	40	31	30

3.6. Catalytic testing

3.6.1. Cracking of n-decane

Cracking of *n*-decane was used as a test reaction to evaluate the intrinsic activity of the pillared materials. Since diffusion limitations are not expected for *n*-decane, the cracking activity of the catalyst should be related to the number and strength of the Brønsted acid sites, with no effect of pore structure or crystal size [5].

Fig. 8 shows the *n*-decane conversion obtained with the three samples at different contact times. The first-order kinetic rate constants are given in Table 4. It can be seen that the activity of the catalysts follows the order MCM36-RT-23 > MCM36-RT-54 > MCM36-HT-24, which correlates very well with the total acidity of the samples as measured by pyridine adsorption–desorption. Indeed, the turnover frequency values (TOF) calculated from the first-order kinetic rate and the concentration of Brønsted acid sites retaining pyridine at 423 K and 523 K give similar values for the three samples (see Table 4). The results indicate that the higher activity of pillared samples obtained by room temperature swell-

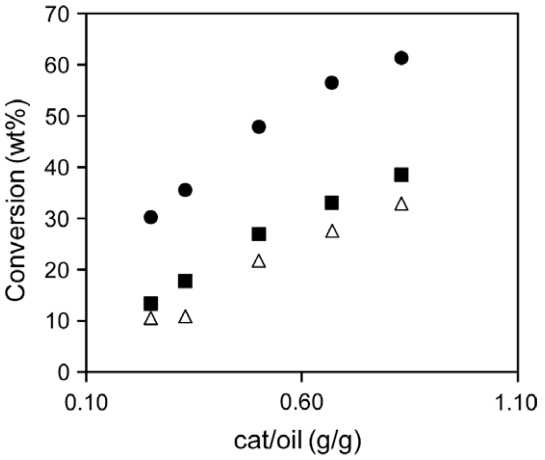

Fig. 8. *n*-Decane cracking. Conversion obtained using MCM36-RT-23 (●), MCM36-RT-54 (■) and MCM36-HT-24 (Δ).

Table 4
First-order kinetic rate constants and turnover frequencies in the *n*-decane cracking at 773 K and 60 s TOS. Selectivities and representative ratios obtained at 35% *n*-decane conversion.

	MCM36-RT-23	MCM36-RT-54	MCM36-HT-24
K (s^{-1}) × 10^2	2.60	1.07	0.82
K/B423 (s^{-1}/mol Py g^{-1}) × 10^4	2.4	1.9	1.3
K/B523 (s^{-1}/mol Py g^{-1}) × 10^4	2.6	2.1	1.7
C1–C4 (wt.%)	22.1	21.2	19.5
C5+ (wt.%)	11.4	10.8	10.5
Coke (wt.%)	1.5	3.0	5.1
Gases composition (wt.%)			
C1 + C2	0.9	1.1	1.0
Propane	4.2	3.4	2.9
Propylene	4.3	4.9	5.2
n-Butane	3.2	2.6	2.1
Isobutane	5.9	5.2	4.1
Total butenes	3.6	4.1	4.2
Isobutene	1.6	1.8	1.8
Ratios			
Propylene/propane	1.02	1.44	1.78
Butenes/butanes	0.39	0.52	0.67
Isobutene/isobutane	0.28	0.34	0.44
(C1 + C2)/isobutane	0.15	0.21	0.23
C3/C4	0.66	0.71	0.79

ing is related to the preservation of a larger amount of zeolite-bridging hydroxyl groups in these materials. Table 4 shows the selectivities to different cracking products obtained with all three pillared materials, as well as some selectivity parameters, such as the olefin to paraffin ratio in the C3 and C4 fractions and the isobutene/isobutane ratio, which give information on the extent of hydrogen transfer that occurs during the cracking process. The higher the above ratios, the lower the extent of hydrogen transfer reactions [31–33]. By taking that into account, it can be seen that MCM36-RT-23 gives the highest hydrogen transfer. This sample is also the one with the highest Brønsted acid site density (Table 3), and therefore it will favor bimolecular reactions like hydrogen transfer to a larger degree [32,34]. Selectivity to gases and liquids is very similar for the three catalysts. The amount of coke is lower with the well-pillared samples due to the presence of 10 MR channels in each layer where coke formation is hindered.

3.6.2. Vacuum gasoil cracking

While *n*-decane cracking measures the intrinsic activity of the material, vacuum gasoil (VGO) cracking activity depends on the accessibility of the bulky hydrocarbon molecules to the acidic sites [5]. Moreover, for the three pillared layered zeolites (for which accessibility to the acidic sites present in the 12MR cups is expected to be similar), one may expect the overall VGO cracking activity to be a function of total concentration of Brønsted acid sites. The results obtained for VGO cracking (Fig. 9) support this hypothesis, since MCM36-RT-23, which has the highest amount of Brønsted acid sites, is the most active sample. The other two samples have very similar acid site density and hence similar activity.

When comparing catalyst selectivity plots (Fig. 9), it can be seen that the most active sample, MCM36-RT-23, is less selective to liquid fuels (gasoline and diesel) and more selective to gases and coke. This is most likely due to higher acid site concentration that results in the secondary cracking of molecules from diesel and gasoline to give gases. Interestingly, when comparing MCM36-RT-54 and MCM36-HT-24, which give very similar activity and have similar acid site concentration, the former is slightly more selective toward gases and coke and less selective toward liquids. A higher degree of structural preservation in MCM36-RT-54 results in less fragmented crystals with lower secondary porosity, possibly increasing recracking of molecules before they can diffuse out from the catalyst, and thus producing more gases and less liquid fuels. The improved structural preservation can also be partially responsible for the high gases production from MCM36-RT-23.

As observed for *n*-decane cracking, the olefin/paraffin ratios in the gaseous products are lowest for MCM36-RT-23 due to a high extent of hydrogen transfer reactions in this sample, owing to its higher density of Brønsted acid sites. This higher hydrogen transfer capacity is in agreement with the higher coke selectivity obtained with this sample.

3.6.3. Xylene isomerization–disproportionation

The isomerization and disproportionation of meta-xylene has been proposed as a test reaction, which gives important information concerning the structure of zeolitic catalysts [18,35–40]. In this reaction, the para-/ortho-xylene ratio depends on the size of the micropores, and on the possible presence of lobes, cages or crossing channels. Moreover, since meta-xylene isomerization is monomolecular, whereas disproportionation is a bimolecular reaction involving a bulkier transition state, the relative extent of these two reactions (isomerization/disproportionation ratio) will indicate the possible presence of void spaces, large enough to allow the bimolecular process to occur.

The initial conversion of meta-xylene over the three pillared samples is shown in Fig. 10. It can be clearly seen that MCM36-RT-23 is again the most active sample due to its high Brønsted acid site density. The other two samples have very similar activity, although a closer look indicates a slightly higher value for MCM36-HT-24. This may be due to easier reactant accessibility as a result of more fragmented structure created by partial dissolution of the crystal during the high-temperature swelling.

It is well known [18,35–40] that the shape and dimensions of the zeolite pores have great influence over the para/ortho selectivity observed during meta-xylene isomerization. The selectivity obtained over medium pore (10MR) zeolites is higher (>2.5) due to differences in the diffusion of both isomers through the narrow channels of these zeolites [41]. On the other hand, the large pore zeolites (12MR) show para/ortho selectivities which are only slightly above the equilibrium value (para/ortho ∼ 1), often in the range of 1.0–1.4 [38]. Zeolites containing both 10MR and 12MR pores show intermediate behavior [12,37]. The three pillared samples analyzed here give para/ortho ratios between 1.4 and 2.0, which are typical of materials containing both medium (10MR) and large pores (12MR) [12,37]. However, MCM36-RT-54 has slightly higher para/ortho ratio (∼2 when compared to ∼1.5 for the other samples), which is very close to that obtained for a MCM-22 material [12]. Minimal structural degradation during the synthesis of this sample results in preservation of 10MR pore channel within the layers, which favors para-xylene production [12]. On the other hand, the para/ortho ratio for MCM36-RT-23 is lowest despite its structural similarity to MCM36-RT-54. This is likely due to the larger number of acid sites in this sample, together with a larger proportion of the sites with strongest acidity, which increases the average lifetime of adsorbed species favoring secondary rearrangement reactions and bringing down the selectivity to para-xylene.

The disproportionation of xylenes to give trimethylbenzene and toluene is a bimolecular secondary reaction, which could be favored by the presence of large cages and high acid site density [42]. Fig. 10 shows that the overall selectivity of all three samples toward isomerization is high (ratio > 10) indicating the predominant effect of the 10MR pores. In the case of MCM36-RT-23, the higher density of acid sites enhances the bimolecular reaction resulting in a lower isomerization to disproportionation ratio [43].

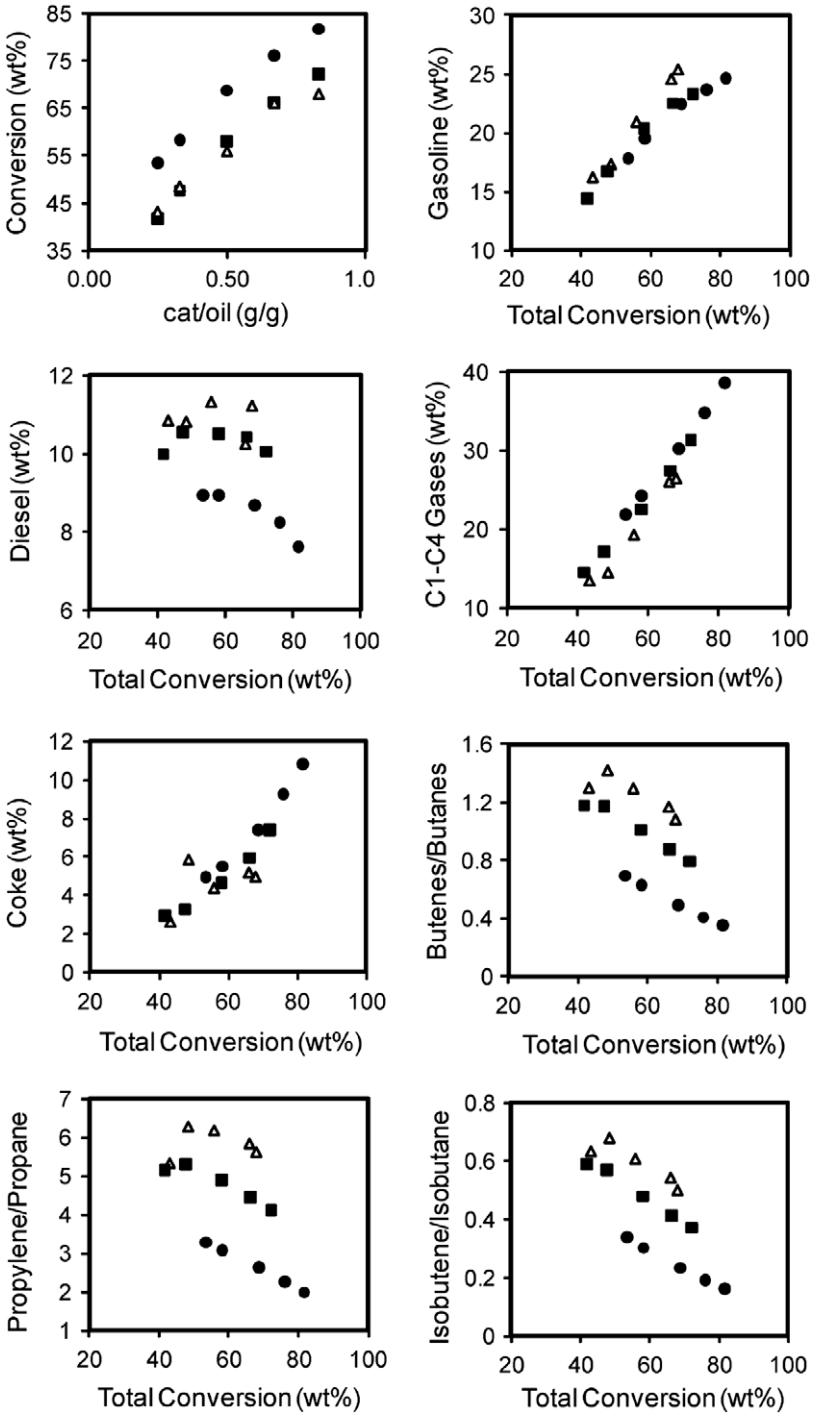

Fig. 9. Vacuum gasoil cracking. Conversion, selectivity and olefin/paraffin ratio in the gas products obtained using MCM36-RT-23 (●), MCM36-RT-54 (■) and MCM36-HT-24 (Δ).

3.6.4. Benzene and toluene alkylation

Aromatics alkylation serves as a useful test reaction to study zeolite topology and is of significant commercial interest in the petrochemical industry [18,37,43,44].

The alkylation of aromatic molecules with propanol occurs through an electrophilic substitution and is considered to proceed via a carbenium ion-type mechanism [45,46]. The alcohol is converted into activated alkene by dehydration on the acid sites of the zeolite. The resulting olefin can follow two major reaction pathways: (1) alkylation with the aromatic, which can further react to give di- and tri-alkyl-aromatics; and (2) oligomerization of the olefin to produce C6 and C9 olefins that can be further transformed through cracking, isomerization and alkylation giving olefins and other alkylbenzenes (toluene, cumene, butylbenzenes, etc.).

The activity and selectivity of the three pillared samples for alkylation of benzene with isopropanol has been obtained at short time on stream (TOS) to minimize the effect of catalyst deactivation. The results presented in Fig. 11 show that MCM36-RT-23 gives the highest benzene conversion in agreement with its high Brønsted acid site density and with the catalytic results reported above. Selectivity to cumene (CUM) is high (between 80% and

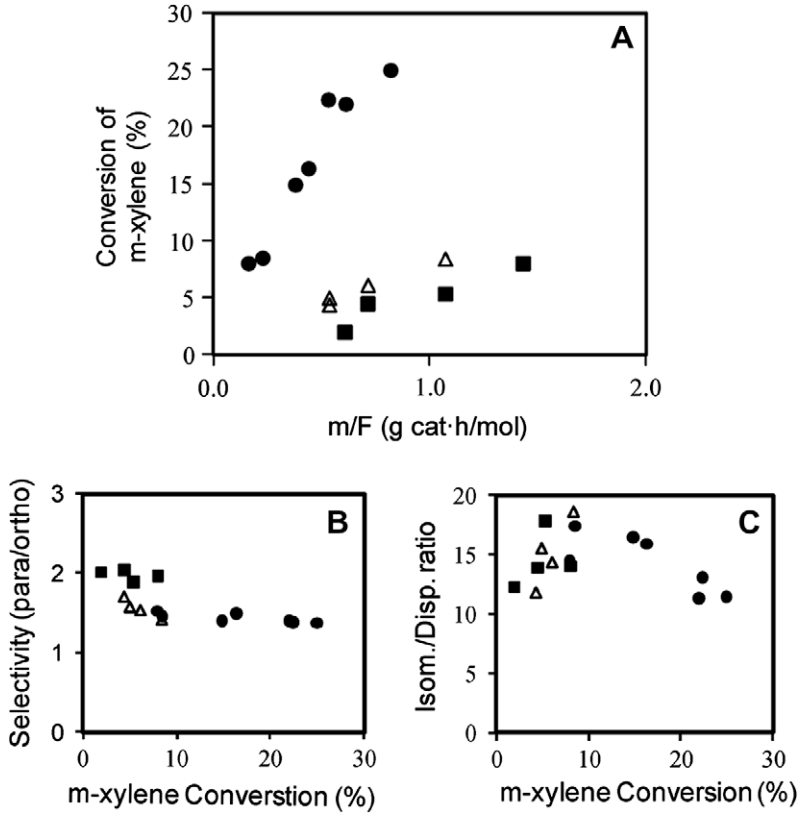

Fig. 10. Meta-xylene isomerization. Conversion (A), selectivity (B) and isomerization/disproportionation ratio (C) obtained using MCM36-RT-23 (●), MCM36-RT-54 (■) and MCM36-HT-24 (Δ).

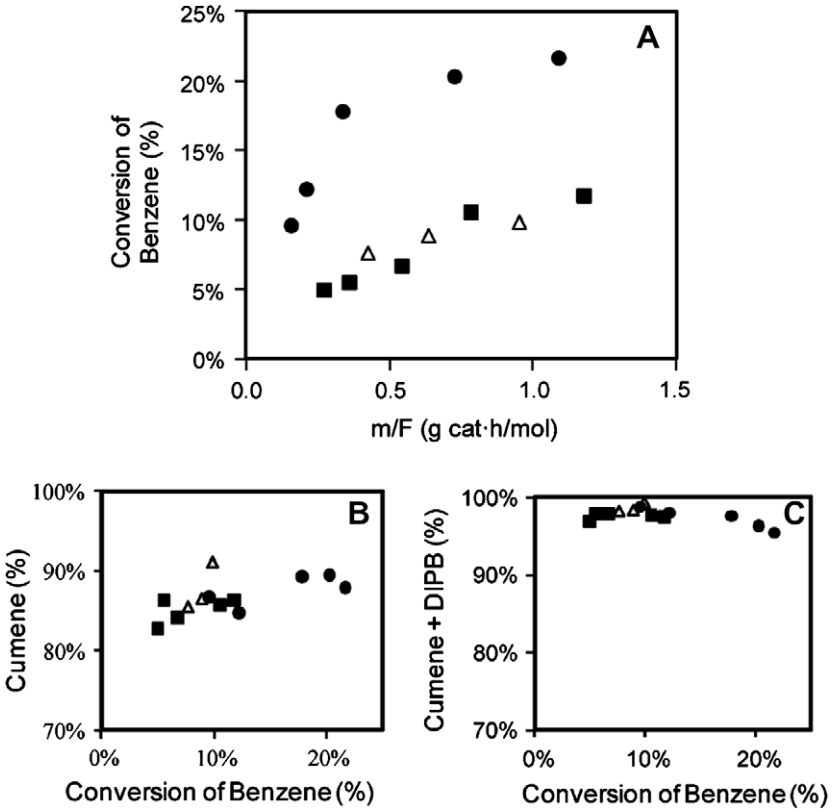

Fig. 11. Alkylation of benzene with isopropanol. Conversion (A), selectivity to cumene (B) and to cumene + DIPB (C) obtained using MCM36-RT-23 (●), MCM36-RT-54 (■) and MCM36-HT-24 (Δ).

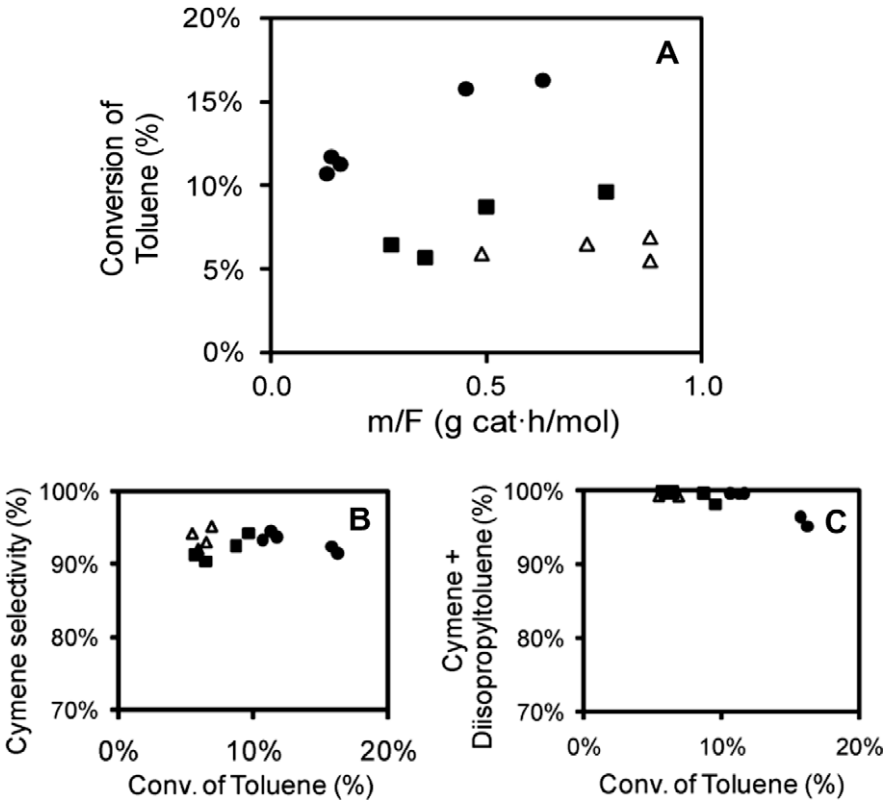

Fig. 12. Alkylation of toluene with isopropanol. Conversion (A), selectivity to cymene (B) and to cymene + DIPT (C) obtained using MCM36-RT-23 (●), MCM36-RT-54 (■) and MCM36-HT-24 (Δ).

90%) for all three samples, and no significant differences are observed. As diisopropylbenzene (DIPB) can be converted to cumene in a second stage of the process by transalkylation with unreacted benzene, it can also be considered as a product of interest. Close to 100% (CUM + DIPB) selectivity values are obtained with all three samples.

Although cumene is the major propylbenzene obtained, undesirable *n*-propylbenzene (NPB) can also be formed by secondary bimolecular transalkylation reactions between cumene and benzene [47,48]. Only traces of NPB are produced under our reaction conditions, as expected from these types of materials with non-crossing 10MR channels.

Results from alkylation of toluene with isopropanol to produce cymene and other products are shown in Fig. 12. The product distribution and trends are very similar to those obtained for benzene alkylation. All three materials show high selectivity to cymene (>90%) and MCM36-RT-23 presents the highest activity due to its higher acid density. Only traces of NPT are formed in our reaction conditions.

4. Conclusions

A modified method to produce MCM-36 materials with higher crystallinity and well-preserved layer structure has been demonstrated. Swelling at room temperature (instead of high temperatures) and extensive washing with water are keys to achieve such high structural integrity in the pillared materials. Elemental analysis, TEM, XRD and nitrogen adsorption revealed that the method preserves overall particle morphology and microporosity within the layers and prevents dissolution of the framework silica. The improved structural preservation is reflected in the acidity and catalytic activity of the resulting pillared materials. The MCM-36 materials prepared by the method presented here exhibit higher Brønsted acid site density and a larger proportion of stronger acidic sites for a given Si/Al ratio, when compared to the one prepared using the method previously reported in the literature. The higher acidity makes these materials very active for a host of catalytic reactions such as cracking, isomerization and alkylation, and better structural preservation affects the product distribution obtained from these reactions.

Acknowledgments

We gratefully acknowledge Sandeep Kumar for the TEM images and Dr. Sonjong Hwang for the NMR spectra of the MCM-36 materials. We thank Professor Frank Bates for his input since the early stages of this work and Professor Aditya Bhan for suggestions during the writing of this manuscript. This work was made possible with the financial support from the NSF (CBET-0403574 (NIRT) and 0327811), and PROMETEO and Consolider from Generalitat Valenciana and Ministerio de Ciencia e Innovación. Parts of this work were carried out in the University of Minnesota I.T. Characterization facility, which receives partial support from the NSF through the NNIN program. M.T. Portilla gratefully acknowledges CSIC for JAE fellowship.

References

[1] C.T. Kresge, W.J. Roth, K.G. Simmons, J.C. Vartuli, WO Patent 92/011935, Mobil Oil Corporation, 1992.
[2] S. Laforge, P. Ayrault, D. Martin, M. Guisnet, Appl. Catal. A 279 (2005) 79.
[3] W.J. Roth, C.T. Kresge, J.C. Vartuli, M.E. Leonowicz, A.S. Fung, S.B. McCullen, Stud. Surf. Sci. Catal. 94 (1995) 301.
[4] J. Kornatowski, J.O. Barth, K. Erdmann, M. Rozwadowski, Micropor. Mesopor. Mater. 90 (2006) 251.
[5] A. Corma, V. Fornes, J. Martinez-Triguero, S.B. Pergher, J. Catal. 186 (1999) 57.
[6] Y.J. He, G.S. Nivarthy, F. Eder, K. Seshan, J.A. Lercher, Micropor. Mesopor. Mater. 25 (1998) 207.
[7] J.-O. Barth, J. Kornatowski, J.A. Lercher, J. Mater. Chem. 12 (2002) 369.

[8] R. Ravishankar, D. Bhattacharya, N.E. Jacob, S. Sivasanker, Micropor. Mater. 4 (1995) 83.
[9] R. Schenkel, J.O. Barth, J. Kornatowski, J.A. Lercher, Stud. Surf. Sci. Catal. 142A (2002) 69.
[10] P. Wu, D. Nuntasri, J. Ruan, Y. Liu, M. He, W. Fan, O. Terasaki, T. Tatsumi, J. Phys. Chem. B 108 (2004) 19126.
[11] S. Maheshwari, E. Jordan, S. Kumar, F.S. Bates, R.L. Penn, D.F. Shantz, M. Tsapatsis, J. Am. Chem. Soc. 130 (2008) 1507.
[12] A. Corma, C. Corell, F. Llopis, A. Martinez, J. Perez-Pariente, Appl. Catal. A 115 (1994) 121.
[13] A. Corma, J.B. Monton, A.V. Orchilles, Appl. Catal. 16 (1985) 59.
[14] R. Kumar, P. Ratnasamy, J. Catal. 116 (1989) 440.
[15] A. Corma, V. Fornes, S.B. Pergher, T.L.M. Maesen, J.G. Buglass, Nature 396 (1998) 353.
[16] C.A. Emeis, J. Catal. 141 (1993) 347.
[17] A. Corma, C. Martinez, F. Ortega, O. Bermudez, Appl. Catal. A 230 (2002) 111.
[18] A. Corma, V.I. Costa-Vaya, M.J. Diaz-Cabanas, F.J. Llopis, J. Catal. 207 (2002) 46.
[19] R. Aiello, F. Crea, F. Testa, G. Demortier, P. Lentz, M. Wiame, J.B. Nagy, Micropor. Mesopor. Mater. 35–36 (2000) 585.
[20] M.A. Camblor, A. Corma, M.-J. Diaz-Cabanas, C. Baerlocher, J. Phys. Chem. B 102 (1998) 44.
[21] G.J. Kennedy, S.L. Lawton, M.K. Rubin, J. Am. Chem. Soc. 116 (1994) 11000.
[22] S.L. Lawton, A.S. Fung, G.J. Kennedy, L.B. Alemany, C.D. Chang, G.H. Hatzikos, D.N. Lissy, M.K. Rubin, H.-K.C. Timken, J. Phys. Chem. 100 (1996) 3788.
[23] W. Kolodziejski, C. Zicovich-Wilson, C. Corell, J. Perez-Pariente, A. Corma, J. Phys. Chem. 99 (1995) 7002.
[24] D. Ma, F. Deng, R. Fu, X. Han, X. Bao, J. Phys. Chem. B 105 (2001) 1770.
[25] S.L. Burkett, M.E. Davis, J. Phys. Chem. B 98 (1994) 4647.
[26] J.C. Groen, S. Abello, L.A. Villaescusa, J. Perez-Ramirez, Micropor. Mesopor. Mater. 114 (2008) 93.
[27] A. Miltenburg, J. Pawlesa, A.M. Bouzga, N. Zilkova, J. Cejka, M. Stoecker, Top. Catal. 52 (2009) 1190.
[28] J.S. Jung, J.W. Park, G. Seo, Appl. Catal. A 288 (2005) 149.
[29] P.P. Man, J. Klinowski, J. Chem. Soc., Chem. Commun. (1988) 1291.
[30] R. Rachwalik, Z. Olejniczak, J. Jiao, J. Huang, M. Hunger, B. Sulikowski, J. Catal. 252 (2007) 161.
[31] J.O. Petunchi, G.A. Sill, W.K. Hall, J. Catal. 141 (1993) 323.
[32] A. Corma, M. Faraldos, A. Martinez, A. Mifsud, J. Catal. 122 (1990) 230.
[33] C. Franco Parra, M.R. Goldwasser, F. Fajula, F. Figueras, Appl. Catal. 17 (1985) 217.
[34] L.A. Pine, P.J. Maher, W.A. Wachter, J. Catal. 85 (1984) 466.
[35] M. Guisnet, N.S. Gnep, S. Morin, Micropor. Mesopor. Mater. 35–36 (2000) 47.
[36] P.A. Jacobs, J.A. Martens, Stud. Surf. Sci. Catal. 28 (1986) 23.
[37] F.J. Llopis, G. Sastre, A. Corma, J. Catal. 227 (2004) 227.
[38] J.A. Martens, J. Perez-Pariente, E. Sastre, A. Corma, P.A. Jacobs, Appl. Catal. 45 (1988) 85.
[39] D.H. Olson, W.O. Haag, ACS Symp. Ser. 248 (1984) 275.
[40] L.B. Young, S.A. Butter, W.W. Kaeding, J. Catal. 76 (1982) 418.
[41] P.B. Weisz, Pure Appl. Chem. 52 (1980) 2091.
[42] J. Perez-Pariente, E. Sastre, V. Fornes, J.A. Martens, P.A. Jacobs, A. Corma, Appl. Catal. 69 (1991) 125.
[43] A. Corma, V. Martinez-Soria, .E. Schnoeveld, J. Catal. 192 (2000) 163.
[44] A. Corma, F.J. Llopis, C. Martinez, G. Sastre, S. Valencia, J. Catal. 268 (2009) 9.
[45] J.R. Anderson, T. Mole, V. Christov, J. Catal. 61 (1980) 477.
[46] Y. Du, H. Wang, S. Chen, J. Mol. Catal. A: Chem. 179 (2002) 253.
[47] J. Cejka, B. Wichterlova, Catal. Rev. – Sci. Eng. 44 (2002) 375.
[48] E.G. Derouane, H. He, S.B.D.-A. Hamid, I.I. Ivanova, Catal. Lett. 58 (1999) 1.